remote sensing

MDPI

Article

Analysis of Long-Term Aerosol Optical Properties Combining AERONET Sunphotometer and Satellite-Based Observations in Hong Kong

Xinyu Yu [1], Janet Nichol [2], Kwon Ho Lee [3], Jing Li [1] and Man Sing Wong [1,4,*]

[1] Department of Land Surveying and Geo-Informatics, The Hong Kong Polytechnic University, Hong Kong, China
[2] Department of Geography, University of Sussex, Brighton BN19RH, UK
[3] Department of Atmospheric & Environmental Sciences, Gangneung-Wonju National University, Gangneung 26403, Korea
[4] Research Institute for Land and Space, The Hong Kong Polytechnic University, Hong Kong, China
* Correspondence: ls.charles@polyu.edu.hk; Tel.: +852-3400-8959

Abstract: This study analyzes seasonal characteristics and long-term variations in aerosol optical parameters in Hong Kong from 2006 to 2021 using AERONET data and satellite-based observations based on the extreme-point symmetric mode decomposition (ESMD) model. The dominant aerosol types in Hong Kong are mixed aerosols and urban/industrial aerosols with fine-mode sizes, and slightly absorbing or non-absorbing properties. Aerosol optical depth (AOD), Angstrom exponent (AE) and single scattering albedo (SSA) varied seasonally with a lower AOD but higher AE and SSA in summer, and elevated AOD but lower AE and SSA in spring and winter. The long-term variations show the year 2012 to be a turning point, with an upward trend in AOD and AE before 2012 and then downwards after 2012. However, for SSA, a rising trend was exhibited in both pre- and post-2012 periods, but with a larger gradient in the first period. The ESMD analysis shows shorter-term, non-linear fluctuations in aerosol optical parameters, with alternating increasing and declining trends. The examination of the relationships between AOD and meteorological factors based on the extreme gradient boosting (XGBoost) method shows that the effects of weather conditions on AOD are complex and non-monotonic. A lower relative humidity, higher wind speed in southwest directions and lower temperature are beneficial to the abatement of aerosol loads in Hong Kong. In conclusion, the findings of this study enhance the understanding of aerosol properties and the interactions between aerosol loading and meteorological factors.

Keywords: seasonal characteristics; aerosol optical parameters; long-term variations; extreme-point symmetric mode decomposition

Citation: Yu, X.; Nichol, J.; Lee, K.H.; Li, J.; Wong, M.S. Analysis of Long-Term Aerosol Optical Properties Combining AERONET Sunphotometer and Satellite-Based Observations in Hong Kong. *Remote Sens.* **2022**, *14*, 5220. https://doi.org/10.3390/rs14205220

Academic Editors: Xingfa Gu, Jing Wei and Shuaiyi Shi

Received: 25 August 2022
Accepted: 15 October 2022
Published: 18 October 2022

1. Introduction

Aerosols are liquid or solid particles of different sizes suspended in the atmosphere, and are emitted from anthropogenic and natural sources. Extensive studies have been conducted to investigate the aerosol distribution and analyze the related effects on climate, the atmospheric environment and human health [1–6]. They can influence the Earth–atmosphere system and climate both indirectly (changing lifetime, amount and radiative properties of cloud by modifying cloud physical properties) and directly (altering the radiative forcing via scattering and absorbing radiation) [7]. Moreover, aerosol leads to considerable uncertainty in Earth–atmosphere interactions and climate change [8]. Thus, quantifying the long-term trends of aerosol parameters and the underlying causes are beneficial to understanding regional air quality conditions and climate variability.

The optical parameters of aerosols, aerosol optical depth (AOD), Angstrom exponent (AE) and single scattering albedo (SSA) indicate some important characteristics of aerosols,

such as column-integrated aerosol loads, particle size and light-absorbing properties. They are also important factors for climate change analysis [9]. AOD is a primary aerosol parameter representing the amount of aerosol loading in the atmosphere and AE is generally used to estimate the aerosol particle size. As suggested by Kaufman [10], coarse-mode aerosols with particle diameters greater than 1 μm are dominant in the atmosphere when the AE value is smaller than 0.7, whereas a higher AE (>1.8) indicates the dominance of fine-mode aerosol with particle diameters smaller than 0.1 μm. An AE value between 0.7 and 1.8 is typical of the accumulation mode and the aerosol diameters vary between 0.1 and 1 μm. SSA indicates the aerosol absorption characteristics, which depend on the chemical composition of the aerosol. Specifically, it measures the ratio of the scattering coefficient to the total extinction coefficient. Currently, the aerosol optical parameters can be acquired from both ground-based and satellite-based measurements. Ground-based observations, such as the Skyradiometer network (SKYNET) [11], Sun-sky radiation observations network (SONET) [12] and Aerosol robotic network (AERONET) [13], provide accurate aerosol measurements with a high temporal resolution. Although some studies have demonstrated that the uneven and sparse distribution limits widespread application (e.g., potential uncertainties in temporal and regional representation) [14,15], the analysis of long-term variations based on the AERONET measurements is still reliable for understanding changes in aerosol characteristics in a specific area.

Numerous studies have been carried out to investigate long-term changes in aerosol properties based on satellite-based and ground-based observations at global or regional scales. For example, Xia [16] suggests that a significant decrease in AOD can be found in Europe and North America by using the data from 79 AERONET stations from 2000 to 2010. By combining multi-source satellite observations, Leeuw et al. [17] observed that AOD trends over mainland China show an initial increase followed by a significant decline between 1995 and 2015. Che et al. [18] analyzed global AOD variations via long-term aerosol datasets and found distinctly different AOD varying trends in different regions. Ramachandran and Rupakheti [19] reveal a rising trend of fine-mode particulate AOD across Asia from 2001 using AERONET data and Moderate resolution Imaging Spectroradiometer (MODIS) observations. Previous studies have mainly focused on exploring variations in AOD, whereas changes in AE and SSA are rarely included, which gives an incomplete view of aerosol variations. Additionally, in the aforementioned studies, variations in aerosol parameters were commonly addressed using the linear regression method. However, the ensemble empirical mode decomposition (EEMD), a non-linear trend analysis method, has been adopted for the estimation of global AOD variations [20]. The results indicated that non-linear varying trends can provide more perceptible changes than linear trends. Therefore, the estimation of long-term variations in aerosol parameters from a non-linear perspective appears a more promising approach.

Basically, changes in aerosol loading are affected by meteorological conditions, and extensive efforts have been made to analyze the correlations [21,22]. Pearson correlation and multiple linear regression (MLR) are commonly used in the above studies to study the associations between AOD and weather conditions. Actually, the effects of meteorological factors on aerosol loading are synergistic and variable. Notably, the aforementioned methods can only derive monotonic relationships. Superior to traditional statistical approaches, machine learning models are capable of estimating the relative importance of driving factors and capturing complex non-linear relationships between predictors and dependent variables. Previous studies have affirmed that when multi-driving variables are involved, it is feasible and reliable to determine the individual impacts of a given factor from synergistic effects on $PM_{2.5}$ pollution using machine learning methods [23,24]. However, to the best of our knowledge, the complex non-monotonic associations of weather conditions with AOD in Hong Kong have not been investigated and interpreted.

Therefore, to fill the aforementioned gaps, and to analyze the impacts of meteorological conditions on AOD, the aerosol parameters measured by the PolyU AERONET station in Hong Kong and the satellite-based observations were integrated and investigated based

on ESMD and a data-driven method (XGBoost). This study was conducted to (1) identify the seasonal characteristics in aerosol optical parameters and the dominant aerosol type in Hong Kong; (2) investigate the long-term variations in AOD, AE and SSA from annual and seasonal perspectives between 2006 and 2021; and (3) reveal how AOD responds to the changes in weather conditions.

2. Materials and Methods

2.1. AERONET Data and Sampling Site

AERONET (https://aeronet.gsfc.nasa.gov/ accessed on 22 August 2022) is a global aerosol monitoring network that provides accurate measurements of aerosol optical parameters at multiple wavelengths [13]. There are three quality levels: Levels 1.0, 1.5 and 2.0, which represent raw observations, cloud-screened data with quality controls but not final calibration, and quality-assured data after pre- and post-field calibrations, respectively. Two AERONET stations are deployed in Hong Kong, namely Sheung and PolyU stations. The Sheung station is a suburban site, while the PolyU station shows subtropical urban aerosol characteristics (22.3033°N, 114.1797°E, 30 m) with a longer service period (starting from November 2005), located on the roof of the Hong Kong Polytechnic University (Figure 1). In this study, daily and monthly Version 3 Level 2.0 AE at 440–675 nm, AOD at 500 nm and Level 1.5 SSA at 440 nm from 2006 to 2021 were adopted. The uncertainty in the obtained AOD is up to 0.02, while SSA is an inversion product with an uncertainty of about 0.03–0.05 [25].

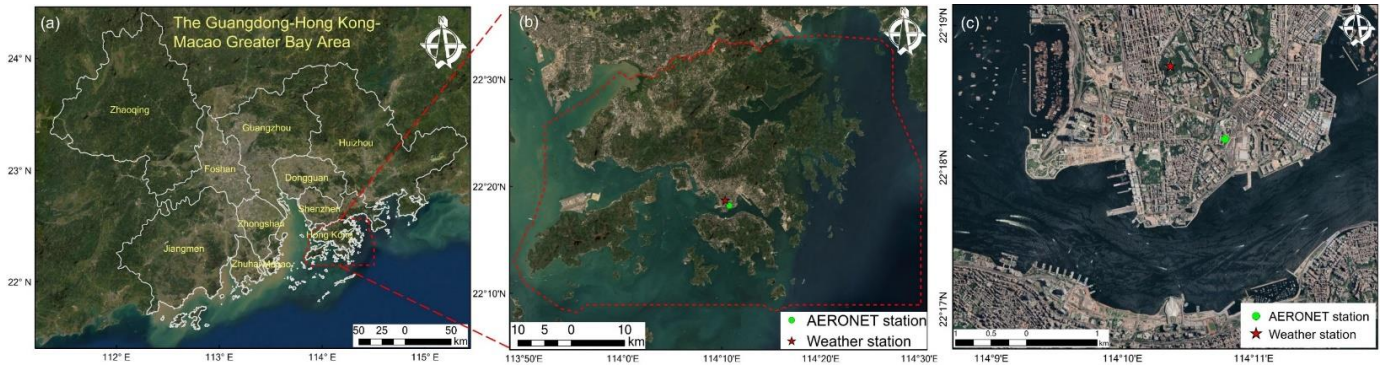

Figure 1. Geographic location of the PolyU AERONET station and King's Park weather station. (**a**) The Guangdong-Hong Kong-Macao Greater Bay Area, (**b**) Hong Kong, and (**c**) enlarged view of the PolyU AERONET station and King's Park weather station location.

2.2. Satellite-Based Observations

Due to the maintenance and calibration of sunphotometers, or weather conditions, missing values of AERONET measurements are inevitable. Therefore, satellite-based observations were considered to ensure continuous time-series sequences. MCD19A2 (https://lpdaac.usgs.gov/ accessed on 22 August 2022), an AOD product at 470 nm and 550 nm wavelengths provided by MODIS with daily intervals and a 1 km spatial resolution via the multi-angle inversion atmospheric correction (MAIAC) approach, was adopted, which is highly consistent with AERONET ground observations [26,27]. A comparison between AERONET AOD measurements and the MODIS MAIAC AOD dataset in different seasons in Hong Kong is displayed in Figure 2. Daily mean satellite-based AOD at 470 nm and 550 nm was extracted by defining with the PolyU AERONET station in the center of an area of 5 × 5 pixels to interpolate the AE at 440–675 nm and AOD at 500 nm according to the equations presented in this section [28]. The results show that the satellite-based observations are in good agreement with the ground-based measurements, with a correlation coefficient from 0.72 to 0.77.

$$\tau(\lambda_i) = \beta\lambda_i^{-\alpha} \quad (1)$$

$$\alpha = -\frac{\ln(\tau_1/\tau_2)}{\ln(\lambda_1/\lambda_2)} \quad (2)$$

where $\tau(\lambda_i)$ represents AOD at λ_i wavelength, α denotes the Angstrom exponent and β is the turbidity coefficient. Subsequently, monthly mean AOD and AE were calculated based on valid daily measurements to complement the missing AERONET data. The percentage of the satellite-based observations used in this study to substitute the AERONET missing data accounts for about 38%.

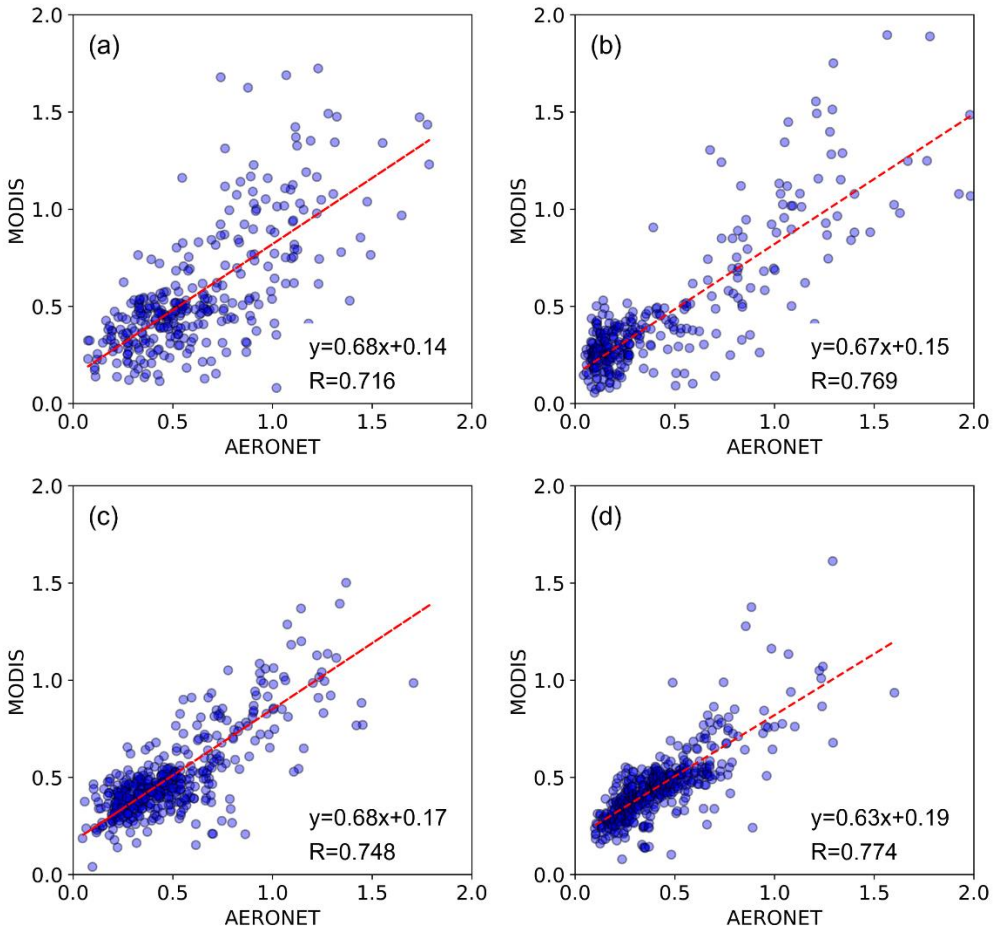

Figure 2. Scatter plots of multi-seasonal MODIS AOD data versus AERONET AOD measurements. (**a**) Spring, (**b**) summer, (**c**) autumn and (**d**) winter. The red dashed line represents the linear regression line.

For the missing values of SSA, the Multi-angle Imaging SpectroRadiometer (MISR) measurements were used, which can provide SSA inversion results with a spatial resolution of 4.4 km and a repeat coverage of about seven to nine days for the sampling site (https://misr.jpl.nasa.gov/ accessed on 22 August 2022). Daily mean SSA at 446 nm was extracted by defining the PolyU AERONET station in the center of an area of 3 × 3 pixels. Some studies have stated that the retrieval SSA of MISR was overestimated as compared to the AERONET, indicating that the effects of some highly absorbing particles were ignored [29–31]. Thus, the retrieved SSA of MISR was corrected by using the SSA inversion results of AERONET using the linear regression. After this, the monthly average SSA was calculated to replace the missing values of AERONET.

2.3. Meteorological Data

In this study, the measurements of the King's Park weather station (22.3119°N, 114.1728°E, 40 m) were used, which is the closest to the PolyU AERONET station (about

1.2 km, red star in Figure 1b). The daily ground-level mean measurements can be acquired from the Hong Kong Observatory, including wind direction, wind speed, relative humidity, temperature, pressure and precipitation (https://www.hko.gov.hk/en/index.html accessed on 22 August 2022). Precipitation was not involved since the ground-level measurements of aerosol optical parameters are not available on rainy days. Additionally, to ensure accuracy and reduce uncertainties, the weather station records consistent with valid measurements of the PolyU AERONET site were extracted and used to explore the impacts of meteorological variables on AOD.

2.4. Extreme-Point Symmetric Mode Decomposition (ESMD)

ESMD was developed based on ensemble empirical mode decomposition (EEMD) [32], which can be used to detect the time-dependent non-linear tendency without antecedent assumption. This is a newly popular approach to probing non-linear varying trends of climate-related issues [33,34]. The original signals can be decomposed into several intrinsic mode functions (IMFs) and a residual curve (R).

$$Y(m) = \sum_{i=1}^{n} M_i(m) + R(m) \quad (3)$$

where $M_i(m)$ is the i^{th} IMF, $R(m)$ is the tendency curve and n denotes the total number of IMFs. More detailed descriptions can be found in the Supplementary Materials. In our study, R denotes the variation tendency of aerosol optical parameters from 2006 to 2021.

2.5. Extreme Gradient Boosting (XGBoost)

XGBoost is an ensemble decision tree model of machine learning with high accuracy for classification and prediction issues. It has been widely applied to explore the relationships between dependent and independent variables. More detailed descriptions can be found in the literature [35]. In this study, XGBoost was adopted to identify the relative importance of meteorological factors and investigate their interactions with AOD, which can be generally demonstrated as follows:

$$y_{AOD} = f(x_i) \quad (4)$$

where y_{AOD} means the daily averaged measurements of the PolyU AERONET station, and x_i represents meteorological factors, including pressure, temperature, wind direction, wind speed and relative humidity.

The relationships between AOD and meteorological factors were estimated by the partial dependence plot results based on the XGBoost model, which can visualize how AOD responds to changes in a specific variable by marginalizing other impact factors [36]. In other words, the variable sensitivity can be illustrated by how the dependent variable reacts when a given predictor changes while other predictors remain constant. To avoid overfitting and to examine reliability, the 10-fold cross-validation (CV) was adopted, whereby the dataset was divided into ten equal-sized subgroups. One subgroup was used as the test dataset and the other samples are for training. The training process is repeated ten times to ensure that every subgroup is tested once. Mean absolute error (MAE), root-mean-square error (RMSE) and the coefficient of determination R-squared (R^2) were used to assess the performance of XGBoost.

3. Results

3.1. Aerosol Optical Characteristics and Aerosol Type Classification

3.1.1. Statistical Description of Aerosol Optical Parameters

Figure 3 displays the multi-seasonal frequency histogram and corresponding statistical descriptions (i.e., minimum, mean, maximum values and standard deviation) based on daily mean measurements. The AOD has a distinct seasonal variation with a unimodal structure (Figure 3a). The lowest and highest daily average AODs occur in summer with values of 0.04 and 1.98, respectively, resulting in the largest standard deviation (SD) of 0.43. Hygroscopic growth and air stagnation may be responsible for the highest AOD

in summer [37]. A much higher AOD was observed in spring, with about 58% of AOD levels above 0.5. Summer, autumn and winter have lower AOD values, especially in summer, when almost 50% of AOD is below 0.3. Thus, spring has the largest mean AOD (0.58), followed by autumn and winter. This may be attributed to long-distance dust and biomass-burning sources, as well as rapid production mechanisms by secondary aerosols [38]. Summer has the lowest mean AOD, as the prevailing wind is southerly in summer, bringing clean air from the South China Sea [39]. Additionally, there is a large amount of rainfall in summer, which can scavenge the pollutants and cleanse the atmosphere [7].

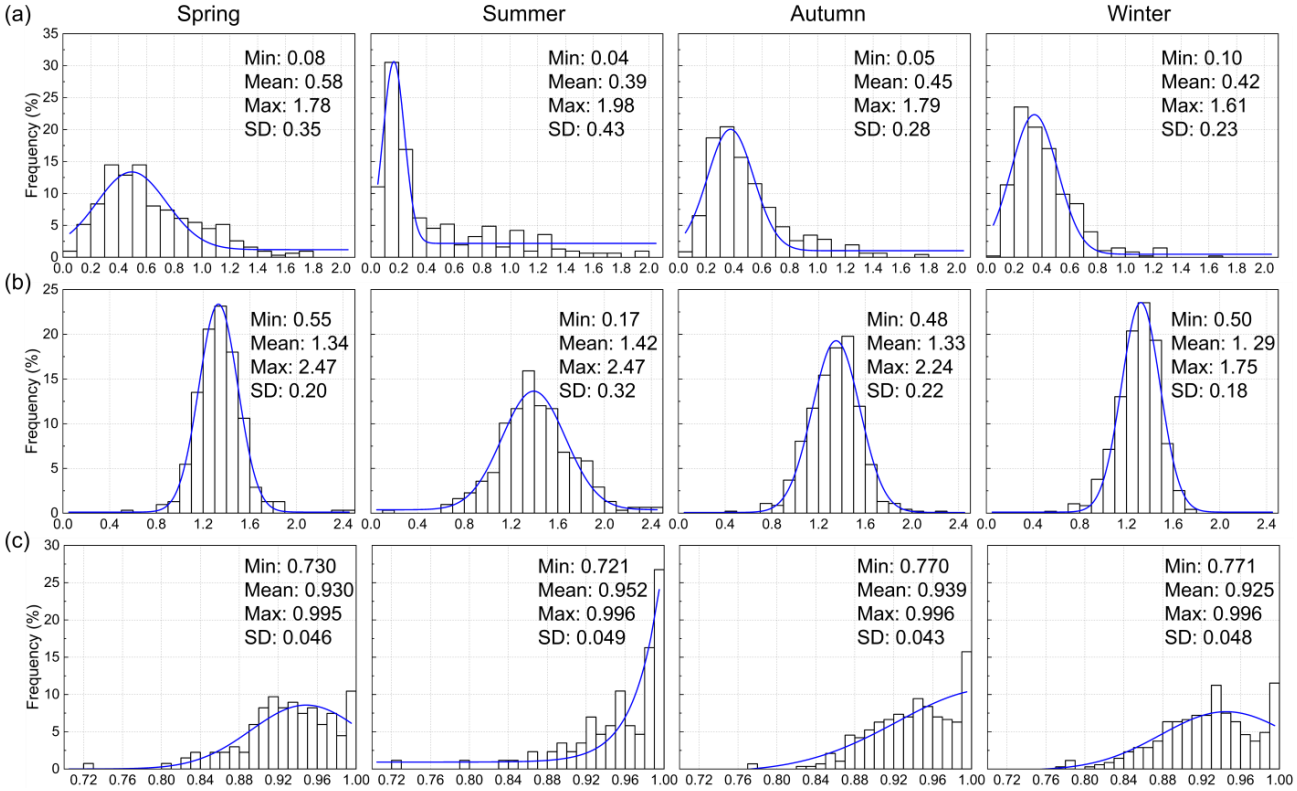

Figure 3. Multi-seasonal frequency histograms of (**a**) AOD, (**b**) AE and (**c**) SSA. The blue line is the fitting curve of the frequency histogram.

Analogously, AE also exhibited a unimodal structure centered at 1.3–1.4 in spring, summer and winter, while centered at 1.4–1.5 in autumn, suggesting the dominance of fine-mode aerosol (Figure 3b). Significant seasonal disparities of AE can be found in summer, with a wide range from 0.17 to 2.47 and a high SD of 0.32. This indicates variations in aerosol particle types in the atmosphere (i.e., fine-mode pollutants and coarse-mode dust). However, Figure 3b suggests that anthropogenic fine-mode particles make more contributions than coarse-mode pollutants over the study period in Hong Kong.

Figure 3c indicates that SSA has a similar distribution frequency histogram in all seasons except summer. The wide range of SSA, 0.721 to 0.996, indicates different aerosol-absorbing characteristics from strongly scattering to strongly absorbing aerosols. A large percentage of high SSA above 0.9 can be observed in all seasons, suggesting that strongly scattering aerosols dominated in Hong Kong during the study period. The highest mean SSA was found in summer, indicating strong scattering properties. This is partly ascribed to the aerosol particles tending to capture atmospheric water vapor under high relative humidity in summer, making a larger particle radius and further increasing the aerosol scattering [40]. Due to the effects of the winter monsoon, the transport of pollutants from China's mainland was facilitated by the prevailing northerly wind [39], and hence absorbing particles (i.e., black carbon) are increased in winter in Hong Kong.

3.1.2. Aerosol Types and Absorbing Aerosol Types

Two different classification criteria suggested by Salinas et al. [41] and Zheng et al. [42] were used to define the aerosol types and absorbing aerosol types in Hong Kong during the study period (see Table 1). For the first one, a daily averaged AOD at 500 nm and AE at 440–675 nm were used to classify the aerosol types, as suggested by Salinas et al. [41]. As depicted in Figure 4a, mixed aerosol (MIXA1 and MIXA2) is the representative type in Hong Kong, accounting for nearly 50%. Instead of pure aerosol, it is composed of different types of aerosol (i.e., dust, urban and biomass burning aerosols). The second dominant type is urban/industrial aerosol (UIA), with a percentage of 33%, followed by biomass-burning aerosol (BBA). Marine aerosol (MA) and dust aerosol (DA) only make up a small fraction (6%). For the second classification criteria, to further explore the dominant aerosol size and properties of absorbing and scattering aerosols, a daily mean Level 2.0 AE at 440–675 nm, fine-mode fraction (FMF) at 500nm and Level 1.5 SSA at 440 nm were used as the aerosol optical parameters, as proposed by Zheng et al. [42]. FMF represents the proportion of fine-mode aerosols in the atmosphere as compared to total aerosols [43,44]. The results are displayed in Figure 4b. Consistent with the above statements, anthropogenic fine-mode aerosols with non-absorbing (FNA) or slight absorbing (FSA) characteristics are the prevailing type in Hong Kong, accounting for over 66% overall. Meanwhile, there are some fine-mode aerosols exhibiting medium (FMA) and highly absorbing (FHA), with percentages of 16.3% and 4.9%, respectively. Marine absorbing (M-A) and non-absorbing aerosols (M-NA) have comparable proportions, 6.5% and 4.8%. The percentage of coarse-mode aerosols is only small (0.7%), and most of them show absorption properties.

Table 1. Classification criteria based on aerosol optical parameters.

	Types	**Aerosol Optical Parameters Thresholds**
Criterion 1 (AOD, AE; Salinas et al. [41])	Marine aerosol (MA)	AOD < 0.2, AE < 1.0
	Dust aerosol (DA)	AOD > 0.2, AE < 1.0
	Mixed aerosol (MIXA1)	AOD < 0.2, AE > 1.0
	Urban/industrial aerosol (UIA)	0.2 < AOD < 0.4, AE > 1.0
	Mixed aerosol (MIXA2)	0.4 < AOD < 0.8, AE > 1.0
	Biomass burning aerosol (BBA)	AOD > 0.8, AE > 1.0
Criterion 2 (AE, SSA, FMF; Zheng et al. [42])	Coarse absorbing (C-A)	SSA < 0.95, AE < 0.6, FMF < 0.4
	Coarse non-absorbing (C-NA)	SSA > 0.95, AE < 0.6, FMF < 0.4
	Mixed absorbing (M-A)	SSA < 0.95, 0.6 < AE < 1.2, 0.4 < FMF < 0.6
	Mixed non-absorbing (M-NA)	SSA > 0.95, 0.6 < AE < 1.2, 0.4 < FMF < 0.6
	Fine highly absorbing (FHA)	SSA < 0.85, AE > 1.2, FMF > 0.6
	Fine medium absorbing (FMA)	0.85 < SSA < 0.9, AE > 1.2, FMF > 0.6
	Fine slightly absorbing (FSA)	0.9 < SSA < 0.95, AE > 1.2, FMF > 0.6
	Fine non-absorbing (FNA)	SSA > 0.95, AE > 1.2, FMF > 0.6

Additionally, seasonal aerosol types and absorbing aerosol types were also investigated to identify the discrepancies between aerosol types in different seasons. As shown in Figure S1, MIXA and UIA are the predominant types in all seasons, and the percentage of UIA in winter is the highest, reaching up to 42.6%. This may be because of the long-range transport of increased urban aerosols during the cold winter heating season in the Chinese mainland [37]. For BBA, it has a higher proportion in spring, possibly caused by frequent forest fires and the increasing burden of biomass burning in spring. The percentages of MA and DA remain relatively constant in different seasons, except in spring, during which MA particles were not found. The seasonal absorbing aerosol types are defined and displayed in Figure S2. Discernible differences occur between summer and winter, with larger quantities of FNA in summer and decreasing frequencies in winter, implying strong scattering properties in summer but more absorption in winter. This is consistent with the statistics of SSA given in Figure 3c. Additionally, there are no significant fluctuations in the percentages of other types (i.e., M-A, M-NA, C-A and C-NA) across different seasons.

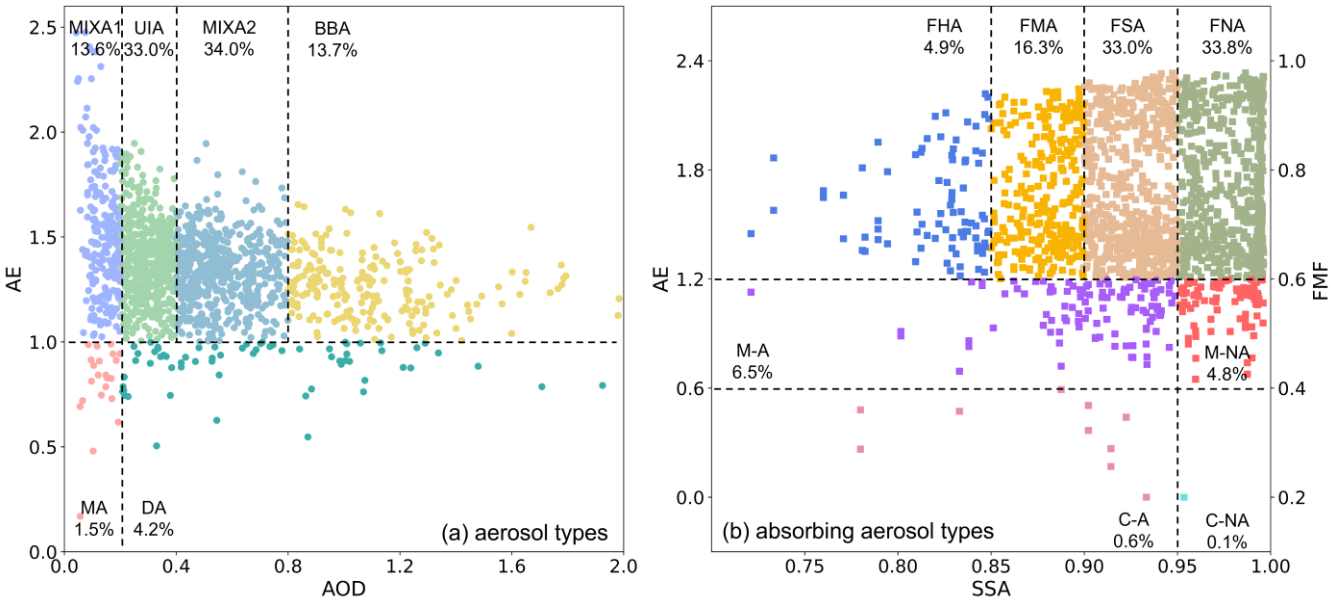

Figure 4. Two aerosol type classification schemes based on the daily measurements of PolyU AERONET station. (**a**) Aerosol types (MIXA: mixed aerosol; BBA: biomass-burning aerosol; MA: marine aerosol; DA: dust aerosol; UIA: urban/industrial aerosol); (**b**) absorbing aerosol types (C-A: coarse absorbing; C-NA: coarse non-absorbing; M-A: mixed absorbing; M-NA: mixed non-absorbing; FSA: fine slightly absorbing; FMA: fine medium absorbing; FHA: fine highly absorbing; FNA: fine non-absorbing).

3.2. Trend Analysis of Aerosol Optical Characteristics

3.2.1. Long-Term Variations of Aerosol Optical Parameters

Figure 5 shows inter-annual varying trends in aerosol optical parameters from 2006 to 2021. The linear and non-linear tendencies were estimated by using monthly averaged measurements of the PolyU AERONET station. The year 2012 can be deemed a turning point with the highest annual mean AOD (0.57). AOD in Hong Kong shows an upward trend before 2012 and a declining trend after 2012 (see Figure S3); additionally, the annual mean AOD decreased gradually and a significant decline trend can be seen for 2012 to 2021, which is consistent with AOD trends in the PRD region suggested by previous studies [45]. Thus, the study period was divided into two subperiods, namely pre-2012 and post-2012. The linear regression shows an increasing tendency in AOD and AE during the pre-2012 period with a significant decreasing trend after 2012 (Figure 5a,b). Contrary to the decrease in AOD and AE, a slight increase in SSA was found, at a rate of 0.0001 during the post-2012 period (Figure 5c).

A time series of aerosol optical parameters were decomposed into five IMFs and one variation trend curve based on the ESMD approach. The variance contribution rate (VCR) and the significance test at 95% confidence level of each IMF and the residual curve were calculated and are displayed in Table 2. It can be seen that the IMFs and trend curves are above the 95% confidence level and significantly correlated with the original time series, except the IMF5 of AOD. As suggested by Zheng et al. [21], the IMFs contain periodic oscillations and irregular non-periodic changes. Take the decomposed results of AOD time series as an example: for the irregular fluctuations (i.e., IMF1 and IMF2 in Figure S4a), the unstable amplitudes of IMFs may be caused by various unexpected factors, including weather conditions, short-term pollution control policies and human activity intensity. Periodic oscillations generally include seasonal (IMF3 in Figure S4a) and inter-annual periodic changes (IMF4 and IMF5 in Figure S4a) related to geographical phenomena. The residual curve can be used to denote the variation trend, which is the main focus of our study. The varying trends analyzed by ESMD are not completely consistent with the linear trends, presenting more fluctuating and detailed variations in aerosol optical parameters. Using AOD as an illustration, the ESMD-based AOD trend (blue dashed line in Figure 4a) shows that there is a decline from 2006 to 2008 with the value changing from above 0.5

to around 0.4, and the values increased subsequently in 2009. The descending trend seen up to 2008 may be caused by emissions control [46] and the reduction in industrial air pollution during the global economic crisis, and an increasing trend can be seen after 2009 since the emissions from economic production and transport returned to pre-recession levels, as suggested by Buchholz et al. [47]. After this, a remarkable descending trend can be found, with the value decreasing to around 0.3 in 2021, which has been attributed to the encouragement of renewable sources of energy and relative air pollution control policies [48,49]. For AE, an increasing tendency similar to the linear trend can be observed before 2012, whereas noticeable fluctuating variations (decreasing–increasing–decreasing) are present in the second period. Especially, there is a steep declining trend after 2020, possibly caused by the reduction in human activities due to the effects of COVID-19 lockdown policies [50]. Nonetheless, most of the monthly averaged AE values are larger than 1.0, suggesting the dominance of anthropogenic aerosols. Figure 5c shows more oscillations in SSA, alternating between upward and downward tendencies. SSA increased substantially after 2017, implying a reduction in absorbing aerosols (long-range transport biomass burning and local vehicles) and more aerosols with strong scattering properties. The underlying cause appears to be the formulation of air pollution control policies and the promotion of new energy sources.

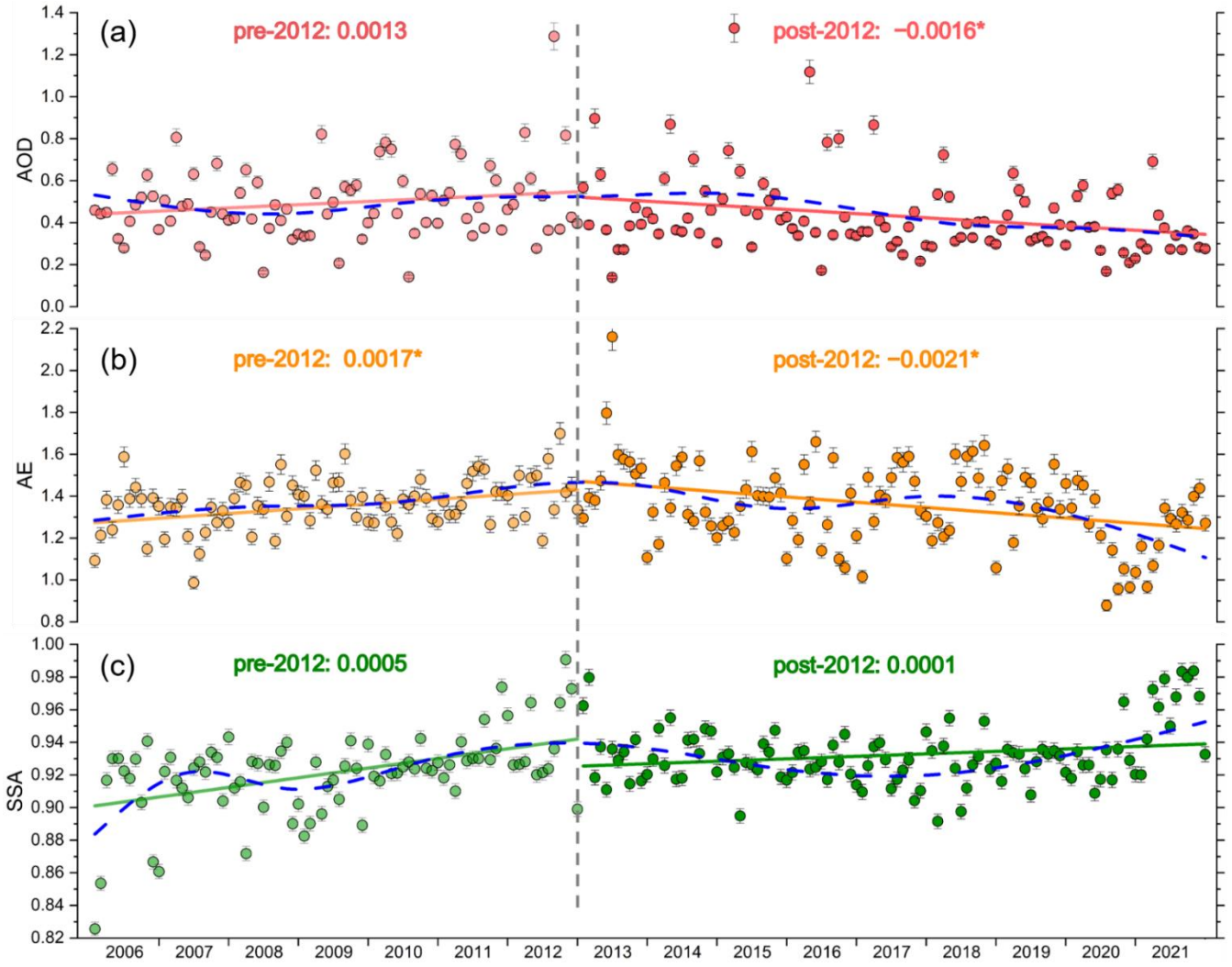

Figure 5. Linear (colored solid lines) and ESMD-based non-linear (blue dashed lines) annual varying trends of (**a**) AOD, (**b**) AE, and (**c**) SSA from 2006 to 2021 based on monthly averaged measurements. (* denotes the linear trends passing the 95% confidence level).

Table 2. Variance contribution rate (VCR) and correlation coefficient of the decomposed results.

Parameters		IMF1	IMF2	IMF3	IMF4	IMF5	R
AOD	VCR (%)	39.36	29.03	14.60	5.04	2.42	9.55
	Correlation coefficient	0.55 *	0.54 *	0.33 *	0.18 *	0.14	0.30 *
AE	VCR (%)	32.52	14.42	27.18	4.47	4.54	16.87
	Correlation coefficient	0.54 *	0.37 *	0.47 *	0.15 *	0.23 *	0.39 *
SSA	VCR (%)	37.97	13.16	9.44	6.53	3.01	29.89
	Correlation coefficient	0.55 *	0.35 *	0.38 *	0.41 *	0.14 *	0.57 *

* represents the significance test at the 95% confidence level.

In conclusion, the linear trend is useful for summarizing the overall variable trends during the study period, whereas the ESMD-based non-linear trends can accurately capture more detailed fluctuations in data, and provide more detailed and plausible variations of aerosol optical properties. The overall results indicate that AOD and AE levels, as well as the proportion of absorbing aerosols in Hong Kong, were reduced during the study period, suggesting that the aforementioned air quality control countermeasures were effective.

3.2.2. Seasonal Variations of Aerosol Optical Parameters

To reveal a detailed pattern of seasonal variations in aerosol optical parameters, linear and ESMD-based non-linear trends were derived using monthly averaged measurements directly. Figure 6a shows that the overall linear seasonal trends in AOD are consistent with the long-term variation directions, but the magnitudes of trends vary in different seasons. For AE, the linear seasonal trends are similar to the long-term variations, except in winter. There is an increase from 2013 to 2021 in winter, attenuating the substantial decline presented in other three seasons and leading to a moderate decrease in the annual trend in the post-2012 period. Similarly, descending variations in linear seasonal trends of SSA are observed in winter, which is different from the increasing pattern in other seasons.

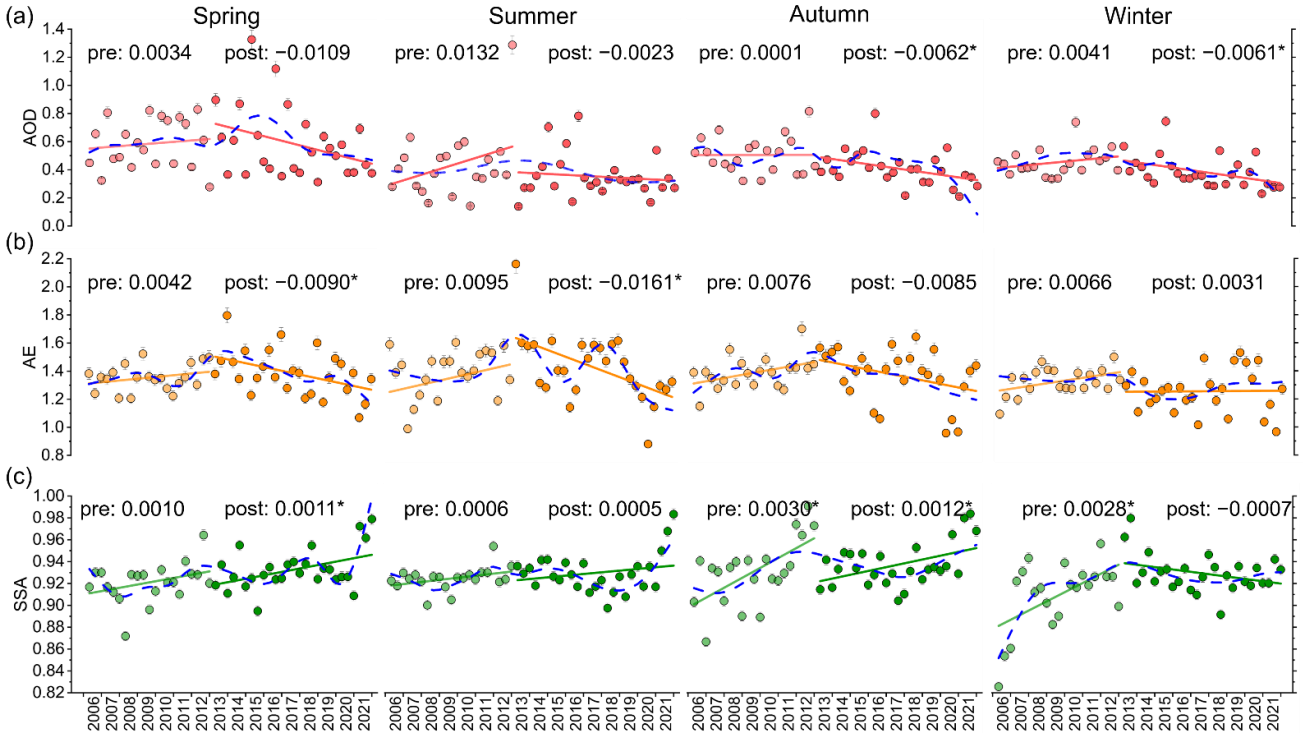

Figure 6. Linear (colored solid lines) and ESMD-based non-linear (blue dashed lines) seasonal varying trends of (**a**) AOD, (**b**) AE, and (**c**) SSA from 2006 to 2021 based on monthly averaged measurements. (* denotes the linear trends passing the 95% confidence level).

A time series of seasonal aerosol optical parameters was also decomposed into several IMFs and the trend curve was based on the ESMD approach. The variance contribution rate (VCR) and the significance test at a 95% confidence level of the varying trends were calculated and are displayed in Table 3, and the estimation results of each IMF are shown in Table S1. The results show that the varying trends are above the 95% confidence level and have a stronger correlation with the original time series, except for the varying trend of summer AOD. For the ESMD-based non-linear trends, these are not entirely aligned with the long-term tendencies shown by the linear analysis. Specifically, in the pre-2012 period, a decreasing–increasing trend of AOD was exhibited in summer and autumn, while a steady upward trend was seen in spring and winter. In terms of the post-2012 period, significant declining trends dominated in all seasons. Strikingly, during the COVID-19 lockdown period (2020–2021), AOD variations leveled off in spring and summer but pronounced decreasing trends occurred in autumn and winter. Apart from the effects of restricted human activities during COVID-19, the reduction in background pollution in Guangdong province is beneficial as well, the upwind area of Hong Kong under winter monsoon [51,52]. Fan et al. [53] also suggested that a considerable mitigation of air pollution can be found across the Pearl River Delta (PRD) area due to the COVID-19 lockdown. As depicted in Figure 6b, spring and autumn have similar changing patterns, with fluctuating variations (increasing–decreasing–increasing) in the pre-2012 period and a continuous downward trend from 2013 to 2021. Although a slightly rising trend in winter AE was presented after 2017, it was offset by the rapid decline in summer AE and a sustained descent in autumn and spring, leading to an overall continuous downward trend in AE after 2017. With regard to the seasonal variations of SSA, the downward trend in spring SSA occurred more frequently, presumably caused by the considerable biomass-burning activities across Indochina Peninsula in spring [54,55]. In addition, during the pre-2012 period, the noticeable increase in winter compensated for the decreasing trend in other seasons, making a similar varying trend to the long-term changes. Although there is a slight descending linear trend in winter SSA during the post-2012 period, a significant rising trend dominated after 2017, indicating a reduction in absorbing aerosols (i.e., black carbon) in recent years. The striking increase in SSA can be found in all seasons from 2020 to 2021, which may be ascribed to the reduction in absorbing aerosols emanating from long-range biomass burning, as well as the restrictions on vehicle transport and human activities during COVID-19 lockdown period [56,57]. Overall, both linear and ESMD-based non-linear seasonal variations of aerosol optical parameters are not completely consistent with the long-term trends. This is because a higher AOD can be observed in spring than in other seasons and spring AOD has been exhibiting a stable trend in recent years. The results imply that attempting to mitigate spring AOD is beneficial to achieving a remarkable drop in overall AOD in Hong Kong.

Table 3. Variance contribution rate (VCR) and correlation coefficient of the residual curve.

		R-Spring	R-Summer	R-Autumn	R-Winter
AOD	VCR (%)	13.03	5.85	35.46	29.60
	Correlation coefficient	0.32 *	0.26	0.47 *	0.49 *
AE	VCR (%)	31.09	36.89	25.01	14.77
	Correlation coefficient	0.50 *	0.58 *	0.44 *	0.29 *
SSA	VCR (%)	37.87	50.98	28.38	48.60
	Correlation coefficient	0.69 *	0.76 *	0.58 *	0.71 *

* represents the significance test at the 95% confidence level.

3.3. Quantitative Impacts of Meteorological Factors

Meteorological conditions are vital influencing factors for AOD, which have non-negligible impacts on the composition and transmission path of aerosols [9]. Pressure (hpa), wind speed (km/h), wind direction (degrees), relative humidity (%), and temperature (°C) are used to quantify the relative contributions of each factor and complex relationships

between explanatory variables and AOD based on the Xgboost model. In our study, after the 10-fold CV test, the XGBoost method achieves an R^2 of 0.80, MAE of 0.08 and RMSE of 0.11. The estimated relative importance of meteorological factors is displayed in Table 4, which is calculated by evaluating the increase in the model prediction error when randomly shuffling a single feature, with the range from 0 to 1 [58]. The results suggest that temperature exerts the greatest influence on AOD, while relative humidity is the second primary influencing factor, followed by wind direction, with an importance rate of about 0.2. Wind speed and pressure make lower contributions to AOD, accounting for 0.18 and 0.16, respectively. Overall, the meteorological variables used in this study have comparable influences in estimating AOD, with a relative importance of around 0.2.

Table 4. Relative importance rate of meteorological factors on AOD.

	Wind Speed	Wind Direction	Relative Humidity	Temperature	Pressure
importance rate	0.18	0.20	0.21	0.25	0.16

Instead of Pearson correlation analysis and multi-linear regression, partial dependence derived by XGBoost was employed to investigate the non-monotonic relationship between a given variable and AOD (Figure 7). The results indicate that AOD increases significantly with relative humidity, increasing from 50% to 70% due to the hygroscopic growth of aerosols [59], whereas there is a noticeable decline in AOD when the relative humidity exceeds 70%. This may be because a higher relative humidity tends to induce frequent precipitation events and the aerosol particles may be scoured, resulting in lower AOD levels [22]. Notably, AOD remains almost unchanged when relative humidity is lower than 50%, which may be responsible for the sparse records of lower relative humidity (see Figure S5), making the correlation insignificant [60]. In contrast, a strong negative correlation can be found between wind speed and AOD, as a higher wind speed promotes aerosol diffusion, dilution and circulation, leading to better air quality [61]. Nonetheless, there are some slight positive trends between wind speed and AOD. This can be attributed to the surface soil and dust raised by high wind speeds, thus increasing the aerosol particles [62]. As depicted in Figure 7c, there is a strong relationship between wind direction and AOD. Specifically, significant upward trends in AOD occur when wind directions change from north to northeast (0–45 degrees) and southwest to west (225–270 degrees). Higher AOD levels can be observed in the northeast (45 degrees) and west (270 degrees) directions. This is more likely caused by the contributions of the long-distance transport of industrial emissions from the mainland (i.e., Henan, Shandong and Anhui provinces) [9], as well as dust and agricultural pollution from Southeast Asia [53]. With the wind directions changing from northeast to east (45–90 degrees) and from west to northwest (270–315 degrees), the neighboring regions (i.e., Guangdong, Fujian and Guangxi provinces) of Hong Kong have cleaner background pollution, leading to a decrease in AOD. The southern part of Hong Kong is surrounded by sea (see Figure 1), which is most likely the reason why AOD remains stable at a wind direction of 90–225 degrees. As can be seen in Figure 7d, AOD is sensitive to variations in temperature, and AOD increases with increased temperature when the temperature is below 25 °C. However, when the temperature is in the range of 28–29 °C, a negative association with AOD is presented. According to the partial dependence results of pressure, AOD is less susceptible to changes in pressure (Figure 7e). AOD decreases gradually with an increasing pressure from 1005 to 1010 hpa, whereas a positive correlation can be observed when the pressure is in the range of 1010–1015 hpa. Subsequently, AOD stabilizes between 0.45 and 0.5 when the pressure exceeds 1015 hpa. In summary, unlike for typical linear correlations, partial dependence analysis implemented by the XGBoost can derive complex and non-linear relationships between AOD and meteorological factors. How AOD responds to the changes in driving factors can be estimated and visualized,

thus recommending the use of black-box models for facilitating the understanding of interactions between AOD and meteorological conditions.

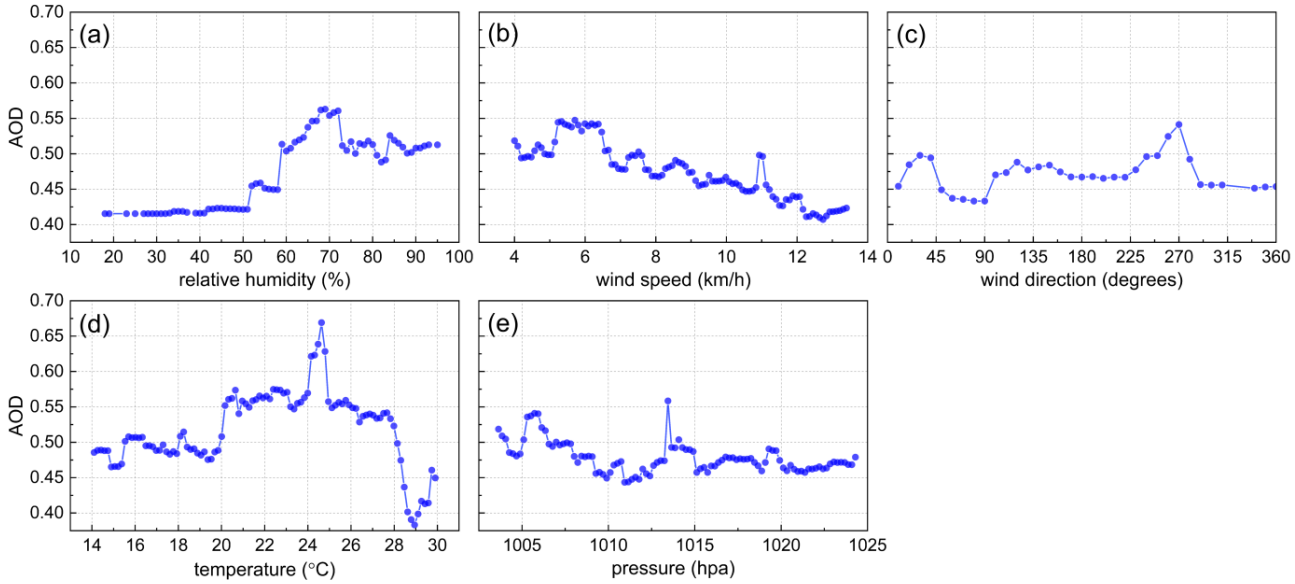

Figure 7. Interactions between AOD and meteorological factors derived by XGBoost.

4. Discussion

Using ground-based AERONET measurements taken over 16 years and combined with satellite-based observations, our study explores the dominant aerosol types, long-term varying trends and the interactions with meteorological factors. The main contributions of our study can be summarized as follows: First, in addition to classifying the aerosol types based on AOD and AE values in previous studies [63–66], the aerosol-absorbing properties in Hong Kong were also categorized using AE, SSA and FMF. Moreover, the multi-seasonal AOD, AE and SSA distribution patterns in Hong Kong were discussed, which provides a basis for understanding the seasonal aerosol optical characteristics in subtropical urban areas such as Hong Kong. Notably, the thresholds of the aerosol optical parameters are generally used for dominant aerosol type classification, while the proportions of specific aerosol types depend on the selected aerosol parameters and the thresholds used for the classification [63]. Additionally, using aerosol optical parameters for aerosol type identification is suitable for areas with a stable aerosol composition, but may not be well-suited for locations with complex topography, Arctic regions and remote marine areas, as aerosols in these regions are difficult to represent using median optical parameters [67]. Second, variations in AOD were mainly analyzed in most previous studies in the literature [16–19], whereas changes in AE and SSA are rarely included, leading to an incomplete view of aerosol variations. Apart from the linear trend, the non-linear fluctuations of aerosol optical parameters were also discussed based on the ESMD method, which can reflect more detailed varying trends. Finally, different from previous studies [21,22], non-monotonic interactions between AOD and meteorological factors were analyzed using a data-driven model, XGBoost, which contributes to the knowledge of how AOD responds to the changes in weather conditions.

However, there are still some limitations in our study. First, the minimum threshold for the number of AERONET AOD observations per day was not considered. To enrich the sample size of the AOD observations, the daily mean AOD was not filtered, although there was only one observation per day. In the future, multi-source AOD datasets (i.e., reanalysis data and satellite-based observations) or more accurately retrieved AOD should be included for the substitute of AERONET AOD to generate accurate and continuous AOD time series. Second, due to the availability of meteorological factors, the interactions between AOD and other meteorological factors (i.e., planetary boundary layer, PBL) were ignored, which

has been suggested to have a significant impact on aerosol vertical distributions and the dispersion of air pollutants in previous studies [68,69].

5. Conclusions

In this study, combining aerosol optical parameters measured by the PolyU AERONET station with satellite observations (i.e., MODIS and MISR aerosol products) from 2006 to 2021 was adopted to analyze the seasonal distribution patterns, varying trends and the association with meteorological factors in Hong Kong. Four primary conclusions can be summarized from the results. Firstly, aerosol optical parameters present significant seasonal characteristics. The seasonal mean AOD is at its highest in spring, while summer has the lowest mean AOD but the largest averaged AE and SSA. Secondly, mixed aerosol and urban/industrial aerosol, which have a fine-mode size with slight or non-absorbing properties, are predominant types in Hong Kong during the study period. Thirdly, the year 2012 can be deemed as the turning point. Both AOD and AE exhibit an increasing trend in the pre-2012 period and a downward tendency after 2012, whereas a consistent rising trend of SSA can be observed over both periods. The use of ESMD to investigate the non-linear annual and seasonal varying trends, was able to provide more detailed insights than linear trends. AOD, AE and SSA present "decreasing (2006–2008)–increasing (2009–2013)–decreasing (2014–2021)", "increasing (2006–2012)–decreasing (2013–2015)-increasing (2016–2018)–decreasing (2019–2021)" and "increasing (2006–2007)–fluctuating (2008–2017)–increasing (2018–2021)" variations during the study period, respectively. Additionally, both linear and ESMD-based non-linear seasonal variations are not completely consistent with the annual trends. The results suggest that the sharp AOD decrease in autumn and winter in recent years contributed to the decline in overall AOD in Hong Kong. Finally, instead of a linear correlation, XGBoost was employed to quantify the non-monotonic relationships between meteorological factors and AOD, as well as rank the relative importance of each variable. It can be concluded that meteorological factors have comparable contributions to AOD and that interactions are complex. The results imply that meteorological conditions with lower relative humidity, higher wind speed, winds from east and southwest directions, lower temperature and higher pressure tend to lower AOD levels. In conclusion, our study can enhance the understanding of aerosol characteristics and long-term variations in Hong Kong. Furthermore, the interactions between meteorological factors and AOD can serve as a basis for developing air quality promotion strategies.

Supplementary Materials: The following supporting information can be downloaded at: https://www.mdpi.com/article/10.3390/rs14205220/s1. Figure S1: Seasonal aerosol types based on daily measurements of the PolyU AERONET station. (a) spring; (b) summer; (c) autumn and (d) winter; Figure S2: Seasonal absorbing aerosol types based on daily measurements of the PolyU AERONET station. (a) spring; (b) summer; (c) autumn and (d) winter; Figure S3: Variations of annual mean AOD with the linear trend (yr-1) in two different periods, namely pre-2012 (red) and post-2012 (blue). * represents the trends passing the 95% confidence level; Figure S4: The decomposed results of aerosol optical parameters based on ESMD. (a) AOD, (b) AE and (c) SSA; Figure S5: Distribution frequency of meteorological factors; Figure S6: Distribution frequency of multi-seasonal meteorological factors; Table S1: Variance contribution rate (VCR, %) and correlation coefficient (CC) of the IMFs.

Author Contributions: Conceptualization, X.Y. and M.S.W.; methodology, X.Y. and M.S.W.; formal analysis, X.Y., M.S.W., J.N., K.H.L. and J.L.; data curation, X.Y.; writing—original draft preparation, X.Y.; writing—review and editing, M.S.W., J.N., K.H.L. and J.L.; supervision, M.S.W., J.N. and K.H.L.; funding acquisition, M.S.W. All authors have read and agreed to the published version of the manuscript.

Funding: This research was funded by the Research Institute for Land and Space (Grant No. 1-CD81), The Hong Kong Polytechnic University; and General Research Fund (Grant No. 15603920 and 15609421), and Collaborative Research Fund (Grant No. C5062-21GF, C7064-18GF), from the Hong Kong Research Grants Council, Hong Kong, China.

Data Availability Statement: All datasets used in this study are available to download by the web links given in the article.

Conflicts of Interest: The authors declare no conflict of interest.

References

1. Kim, M.; Kim, J.; Wong, M.S.; Yoon, J.; Lee, J.; Wu, D.; Chan, P.; Nichol, J.E.; Chung, C.-Y.; Ou, M.L. Improvement of aerosol optical depth retrieval over Hong Kong from a geostationary meteorological satellite using critical reflectance with background optical depth correction. *Remote Sens. Environ.* **2014**, *142*, 176–187. [CrossRef]
2. Wong, M.S.; Lee, K.H.; Nichol, J.E.; Li, Z. Retrieval of Aerosol Optical Thickness Using MODIS 500 × 500 m^2, a Study in Hong Kong and the Pearl River Delta Region. *IEEE Trans. Geosci. Remote Sens.* **2010**, *48*, 3318–3327. [CrossRef]
3. Wong, M.S.; Nichol, J.E.; Lee, K.H. An operational MODIS aerosol retrieval algorithm at high spatial resolution, and its application over a complex urban region. *Atmos. Res.* **2011**, *99*, 579–589. [CrossRef]
4. Huebert, B.J.; Bates, T.; Russell, P.B.; Shi, G.; Kim, Y.J.; Kawamura, K.; Carmichael, G.; Nakajima, T. An overview of ACE-Asia: Strategies for quantifying the relationships between Asian aerosols and their climatic impacts. *J. Geophys. Res. Atmos.* **2003**, *108*, 8633. [CrossRef]
5. Sheesley, R.J.; Schauer, J.J.; Chowdhury, Z.; Cass, G.R.; Simoneit, B.R. Characterization of organic aerosols emitted from the combustion of biomass indigenous to South Asia. *J. Geophys. Res. Atmos.* **2003**, *108*, 4285. [CrossRef]
6. Pye, H.O.; Ward-Caviness, C.K.; Murphy, B.N.; Appel, K.W.; Seltzer, K.M. Secondary organic aerosol association with cardiorespiratory disease mortality in the United States. *Nat. Commun.* **2021**, *12*, 5721. [CrossRef] [PubMed]
7. Wang, Z.; Liu, D.; Wang, Z.; Wang, Y.; Khatri, P.; Zhou, J.; Takamura, T.; Shi, G. Seasonal characteristics of aerosol optical properties at the SKYNET Hefei site (31.90 N, 117.17 E) from 2007 to 2013. *J. Geophys. Res. Atmos.* **2014**, *119*, 6128–6139. [CrossRef]
8. IPCC. Climate change 2013: The physical science basis. In *Contribution of Working Group I to the Fifth Assessment*; Stocker, T.F., Qin, D., Plattner, G.K., Tignor, M.M.H.L., Allen, S.K., Boschung, J., Nauels, A., Xia, Y., Midgley, P.M., Eds.; Cambridge University Press: Cambridge, UK; New York, NY, USA, 2013; p. 1535.
9. Deng, X.; Shi, C.; Wu, B.; Chen, Z.; Nie, S.; He, D.; Zhang, H. Analysis of aerosol characteristics and their relationships with meteorological parameters over Anhui province in China. *Atmos. Res.* **2012**, *109*, 52–63. [CrossRef]
10. Kaufman, Y.J. Remote sensing of direct and indirect aerosol forcing. In *Aerosol Forcing of Climate*; Charlson, R.J., Heintzenberg, J., Eds.; John Wiley: New York, NY, USA, 1995; pp. 297–332.
11. Nakajima, T.; Campanelli, M.; Che, H.; Estellés, V.; Irie, H.; Kim, S.W.; Kim, J.; Liu, D.; Nishizawa, T.; Pandithurai, G.; et al. An overview of and issues with sky radiometer technology and SKYNET. *Atmos. Meas. Tech.* **2020**, *13*, 4195–4218. [CrossRef]
12. Li, Z.Q.; Xu, H.; Li, K.T.; Li, D.H.; Xie, Y.S.; Li, L.; Zhang, Y.; Gu, X.F.; Zhao, W.; Tian, Q.J.; et al. Comprehensive study of optical, physical, chemical, and radiative properties of total columnar atmospheric aerosols over China: An overview of Sun–Sky Radiometer Observation Network (SONET) measurements. *Bull. Am. Meteorol. Soc.* **2018**, *99*, 739–755. [CrossRef]
13. Holben, B.N.; Eck, T.F.; Slutsker, I.A.; Tanre, D.; Buis, J.P.; Setzer, A.; Vermote, E.; Reagan, J.A.; Kaufman, Y.J.; Nakajima, T.; et al. AERONET—A federated instrument network and data archive for aerosol characterization. *Remote Sens. Environ.* **1998**, *66*, 1–16. [CrossRef]
14. Kinne, S.; Lohmann, U.; Feichter, J.; Schulz, M.; Timmreck, C.; Ghan, S.; Easter, R.; Chin, M.; Ginoux, P.; Takemura, T.; et al. Monthly averages of aerosol properties: A global comparison among models, satellite data, and AERONET ground data. *J. Geophys. Res. Atmos.* **2003**, *108*, 4634. [CrossRef]
15. Li, J.; Liu, L.; Lacis, A.A.; Carlson, B.E. An optimal fitting approach to improve the GISS ModelE aerosol optical property parameterization using AERONET data. *J. Geophys. Res. Atmos.* **2010**, *115*, D16211. [CrossRef]
16. Xia, X. Variability of aerosol optical depth and Angstrom wavelength exponent derived from AERONET observations in recent decades. *Environ. Res. Lett.* **2011**, *6*, 044011. [CrossRef]
17. De Leeuw, G.; Sogacheva, L.; Rodriguez, E.; Kourtidis, K.; Georgoulias, A.K.; Alexandri, G.; Amiridis, V.; Proestakis, E.; Marinou, E.; Xue, Y.; et al. Two decades of satellite observations of AOD over mainland China using ATSR-2, AATSR and MODIS/Terra: Data set evaluation and large-scale patterns. *Atmos. Chem. Phys.* **2018**, *18*, 1573–1592. [CrossRef]
18. Che, H.; Gui, K.; Xia, X.; Wang, Y.; Holben, B.N.; Goloub, P.; Cuevas-Agulló, E.; Wang, H.; Zheng, Y.; Zhao, H.; et al. Large contribution of meteorological factors to inter-decadal changes in regional aerosol optical depth. *Atmos. Chem. Phys.* **2019**, *19*, 10497–10523. [CrossRef]
19. Ramachandran, S.; Rupakheti, M. Trends in the types and absorption characteristics of ambient aerosols over the Indo-Gangetic Plain and North China Plain in last two decades. *Sci. Total Environ.* **2022**, *831*, 154867. [CrossRef]
20. Zhang, Z.Y.; Wong, M.S.; Nichol, J. Global trends of aerosol optical thickness using the ensemble empirical mode decomposition method. *Int. J. Climatol.* **2016**, *36*, 4358–4372. [CrossRef]
21. Zheng, Y.; Wang, X.; Zhang, X.; Hu, G. Multi-spatiotemporal patterns of aerosol optical depth and influencing factors during 2000–2020 from two spatial perspectives: The entire Yellow River Basin region and its urban agglomerations. *Int. J. Appl. Earth Obs. Geoinf.* **2022**, *106*, 102643. [CrossRef]
22. He, L.; Wang, L.; Huang, B.; Wei, J.; Zhou, Z.; Zhong, Y. Anthropogenic and meteorological drivers of 1980–2016 trend in aerosol optical and radiative properties over the Yangtze River Basin. *Atmos. Environ.* **2020**, *223*, 117188. [CrossRef]

23. Zhang, Z.; Xu, B.; Xu, W.; Wang, F.; Gao, J.; Li, Y.; Li, M.; Feng, Y.; Shi, G. Machine learning combined with the PMF model reveal the synergistic effects of sources and meteorological factors on $PM_{2.5}$ pollution. *Environ. Res.* **2022**, *212*, 113322. [CrossRef] [PubMed]
24. Yang, N.; Shi, H.; Tang, H.; Yang, X. Geographical and temporal encoding for improving the estimation of $PM_{2.5}$ concentrations in China using end-to-end gradient boosting. *Remote Sens. Environ.* **2022**, *269*, 112828. [CrossRef]
25. Dubovik, O.; Smirnov, A.; Holben, B.N.; King, M.D.; Kaufman, Y.J.; Eck, T.F.; Slutsker, I. Accuracy assessments of aerosol optical properties retrieved from Aerosol Robotic Network (AERONET) Sun and sky radiance measurements. *J. Geophys. Res. Atmos.* **2000**, *105*, 9791–9806. [CrossRef]
26. Lyapustin, A.; Martonchik, J.; Wang, Y.; Laszlo, I.; Korkin, S. Multiangle implementation of atmospheric correction (MAIAC): 1. Radiative transfer basis and look-up tables. *J. Geophys. Res. Atmos.* **2011**, *116*, D03210. [CrossRef]
27. Tao, M.; Wang, J.; Li, R.; Wang, L.; Wang, L.; Wang, Z.; Tao, J.; Che, H.; Chen, L. Performance of MODIS high-resolution MAIAC aerosol algorithm in China: Characterization and limitation. *Atmos. Environ.* **2019**, *213*, 159–169. [CrossRef]
28. Ångström, A. On the atmospheric transmission of sun radiation and on dust in the air. *Geogr. Ann.* **1929**, *11*, 156–166. [CrossRef]
29. Kahn, R.A.; Gaitley, B.J. An analysis of global aerosol type as retrieved by MISR. *J. Geophys. Res. Atmos.* **2015**, *120*, 4248–4281. [CrossRef]
30. Si, Y.; Li, S.; Chen, L.; Shang, H.; Wang, L.; Letu, H. Assessment and improvement of MISR Angstrom exponent and single-scattering albedo products using AERONET data in China. *Remote Sens.* **2017**, *9*, 693. [CrossRef]
31. Kahn, R.A.; Gaitley, B.J.; Garay, M.J.; Diner, D.J.; Eck, T.F.; Smirnov, A.; Holben, B.N. Multiangle Imaging SpectroRadiometer global aerosol product assessment by comparison with the Aerosol Robotic Network. *J. Geophys. Res. Atmos.* **2010**, *115*, D23209. [CrossRef]
32. Wang, J.L.; Li, Z.J. Extreme-point symmetric mode decomposition method for data analysis. *Adv. Adapt. Data Anal.* **2013**, *5*, 1350015. [CrossRef]
33. Qin, Y.; Li, B.; Chen, Z.; Chen, Y.; Lian, L. Spatio-temporal variations of nonlinear trends of precipitation over an arid region of northwest China according to the extreme-point symmetric mode decomposition method. *Int. J. Climatol.* **2018**, *38*, 2239–2249. [CrossRef]
34. Wang, X.; Chen, Y.; Li, Z.; Fang, G.; Wang, F.; Liu, H. The impact of climate change and human activities on the Aral Sea Basin over the past 50 years. *Atmos. Res.* **2020**, *245*, 105125. [CrossRef]
35. Chen, T.; Guestrin, C. XGBoost: A Scalable Tree Boosting System. In Proceedings of the 22nd ACM SIGKDD International Conference on Knowledge Discovery and Data Mining, San Francisco, CA, USA, 13–17 August 2016; pp. 785–794. [CrossRef]
36. Friedman, J.H. Greedy function approximation: A gradient boosting machine. *Ann. Stat.* **2001**, *29*, 1189–1232. [CrossRef]
37. Yu, X.; Lü, R.; Liu, C.; Yuan, L.; Shao, Y.; Zhu, B.; Lei, L. Seasonal variation of columnar aerosol optical properties and radiative forcing over Beijing, China. *Atmos. Environ.* **2017**, *166*, 340–350. [CrossRef]
38. Kumar, K.R.; Kang, N.; Sivakumar, V.; Griffith, D. Temporal characteristics of columnar aerosol optical properties and radiative forcing (2011–2015) measured at AERONET's Pretoria_CSIR_DPSS site in South Africa. *Atmos. Environ.* **2017**, *165*, 274–289. [CrossRef]
39. Liu, Y.; He, J.; Lai, X.; Zhang, C.; Zhang, L.; Gong, S.; Che, H. Influence of atmospheric circulation on aerosol and its optical characteristics in the pearl river delta region. *Atmosphere* **2020**, *11*, 288. [CrossRef]
40. Xia, X.; Che, H.; Zhu, J.; Chen, H.; Cong, Z.; Deng, X.; Fan, X.; Fu, Y.; Goloub, P.; Jiang, H.; et al. Ground-based remote sensing of aerosol climatology in China: Aerosol optical properties, direct radiative effect and its parameterization. *Atmos. Environ.* **2016**, *124*, 243–251. [CrossRef]
41. Salinas, S.V.; Chew, B.N.; Liew, S.C. Retrievals of aerosol optical depth and Ångström exponent from ground-based Sun-photometer data of Singapore. *Appl. Opt.* **2009**, *48*, 1473–1484. [CrossRef]
42. Zheng, C.; Zhao, C.; Zhu, Y.; Wang, Y.; Shi, X.; Wu, X.; Chen, T.; Wu, F.; Qiu, Y. Analysis of influential factors for the relationship between $PM_{2.5}$ and AOD in Beijing. *Atmos. Chem. Phys.* **2017**, *17*, 13473–13489. [CrossRef]
43. Bellouin, N.; Boucher, O.; Haywood, J.; Reddy, M.S. Global estimate of aerosol direct radiative forcing from satellite measurements. *Nature* **2005**, *438*, 1138–1141. [CrossRef] [PubMed]
44. Yan, X.; Zang, Z.; Li, Z.; Luo, N.; Zuo, C.; Jiang, Y.; Li, D.; Guo, Y.; Zhao, W.; Shi, W.; et al. A global land aerosol fine-mode fraction dataset (2001–2020) retrieved from MODIS using hybrid physical and deep learning approaches. *Earth Syst. Sci. Data* **2022**, *14*, 1193–1213. [CrossRef]
45. Zhang, L.; Zhang, M.; Yao, Y. Multi-time scale analysis of regional aerosol optical depth changes in national-level urban agglomerations in China using modis collection 6.1 datasets from 2001 to 2017. *Remote Sens.* **2019**, *11*, 201. [CrossRef]
46. Cai, S.; Wang, Y.; Zhao, B.; Wang, S.; Chang, X.; Hao, J. The impact of the "air pollution prevention and control action plan" on $PM_{2.5}$ concentrations in Jing-Jin-Ji region during 2012–2020. *Sci. Total Environ.* **2017**, *580*, 197–209. [CrossRef] [PubMed]
47. Buchholz, R.R.; Worden, H.M.; Park, M.; Francis, G.; Deeter, M.N.; Edwards, D.P.; Emmons, L.K.; Gaubert, B.; Gille, J.; Martínez-Alonso, S.; et al. Air pollution trends measured from Terra: CO and AOD over industrial, fire-prone, and background regions. *Remote Sens. Environ.* **2021**, *256*, 112275. [CrossRef]
48. Zhang, Q.; He, K.; Huo, H. Cleaning China's air. *Nature* **2012**, *484*, 161–162. [CrossRef]
49. Hong Kong Environmental Protection Department (HKEPD). Air Pollution Control Strategies. 2019. Available online: https://www.epd.gov.hk/epd/english/environmentinhk/air/prob_solutions/strategies_apc.html (accessed on 22 August 2022).

50. Wang, S.; Zhang, Y.; Ma, J.; Zhu, S.; Shen, J.; Wang, P.; Zhang, H. Responses of decline in air pollution and recovery associated with COVID-19 lockdown in the Pearl River Delta. *Sci. Total Environ.* **2021**, *756*, 143868. [CrossRef]
51. Zeren, Y.; Guo, H.; Lyu, X.; Zhou, B.; Liu, X.; Yang, L.; Yuan, Z.; Wang, Y. Remarkable spring increase overwhelmed hard-earned autumn decrease in ozone pollution from 2005 to 2017 at a suburban site in Hong Kong, South China. *Sci. Total Environ.* **2022**, *831*, 154788. [CrossRef]
52. Jiang, F.; Guo, H.; Wang, T.J.; Cheng, H.R.; Wang, X.M.; Simpson, I.J.; Ding, A.; Saunders, S.M.; Lam, S.H.M.; Blake, D.R. An ozone episode in the Pearl River Delta: Field observation and model simulation. *J. Geophys. Res. Atmos.* **2010**, *115*, D22305. [CrossRef]
53. Fan, L.; Fu, S.; Wang, X.; Fu, Q.; Jia, H.; Xu, H.; Qin, G.; Hu, X.; Cheng, J. Spatiotemporal variations of ambient air pollutants and meteorological influences over typical urban agglomerations in China during the COVID-19 lockdown. *J. Environ. Sci.* **2021**, *106*, 26–38. [CrossRef]
54. Liao, Z.; Ling, Z.; Gao, M.; Sun, J.; Zhao, W.; Ma, P.; Quan, J.; Fan, S.; Liao, Z.; Ling, Z.; et al. Tropospheric ozone variability over Hong Kong based on recent 20 years (2000–2019) ozonesonde observation. *J. Geophys. Res. Atmos.* **2021**, *126*, e2020JD033054. [CrossRef]
55. Xue, L.; Ding, A.; Cooper, O.; Huang, X.; Wang, W.; Zhou, D.; Wu, Z.; McClure-Begley, A.; Petropavlovskikh, I.; Andreae, M.O.; et al. ENSO and Southeast Asian biomass burning modulate subtropical trans-Pacific ozone transport. *Natl. Sci. Rev.* **2021**, *8*, nwaa132. [CrossRef]
56. Jia, M.; Evangeliou, N.; Eckhardt, S.; Huang, X.; Gao, J.; Ding, A.; Stohl, A. Black carbon emission reduction due to COVID-19 lockdown in China. *Geophys. Res. Lett.* **2021**, *48*, e2021GL093243. [CrossRef]
57. Lin, Y.C.; Zhang, Y.L.; Xie, F.; Fan, M.Y.; Liu, X. Substantial decreases of light absorption, concentrations and relative contributions of fossil fuel to light-absorbing carbonaceous aerosols attributed to the COVID-19 lockdown in east China. *Environ. Pollut.* **2021**, *275*, 116615. [CrossRef] [PubMed]
58. Casalicchio, G.; Molnar, C.; Bischl, B. Visualizing the feature importance for black box models. In Proceedings of the Joint European Conference on Machine Learning and Knowledge Discovery in Databases, Würzburg, Germany, 16–20 September 2018; Springer: Cham, Switzerland; pp. 655–670.
59. Malm, W.C.; Day, D.E. Estimates of aerosol species scattering characteristics as a function of relative humidity. *Atmos. Environ.* **2001**, *35*, 2845–2860. [CrossRef]
60. Zhu, X.; Li, Y.; Wang, X. Machine learning prediction of biochar yield and carbon contents in biochar based on biomass characteristics and pyrolysis conditions. *Bioresour. Technol.* **2019**, *288*, 121527. [CrossRef] [PubMed]
61. Tai, A.P.; Mickley, L.J.; Jacob, D.J. Correlations between fine particulate matter ($PM_{2.5}$) and meteorological variables in the United States: Implications for the sensitivity of $PM_{2.5}$ to climate change. *Atmos. Environ.* **2010**, *44*, 3976–3984. [CrossRef]
62. Csavina, J.; Field, J.; Félix, O.; Corral-Avitia, A.Y.; Sáez, A.E.; Betterton, E.A. Effect of wind speed and relative humidity on atmospheric dust concentrations in semi-arid climates. *Sci. Total Environ.* **2014**, *487*, 82–90. [CrossRef]
63. Liu, Y.; Yi, B. Aerosols over East and South Asia: Type identification, optical properties, and implications for radiative forcing. *Remote Sens.* **2022**, *14*, 2058. [CrossRef]
64. Cúneo, L.; Ulke, A.G.; Cerne, B. Advances in the characterization of aerosol optical properties using long-term data from AERONET in Buenos Aires. *Atmos. Pollut. Res.* **2022**, *13*, 101360. [CrossRef]
65. Stefan, S.; Voinea, S.; Iorga, G. Study of the aerosol optical characteristics over the Romanian Black Sea Coast using AERONET data. *Atmos. Pollut. Res.* **2020**, *11*, 1165–1178. [CrossRef]
66. Ozdemir, E.; Tuygun, G.T.; Elbir, T. Application of aerosol classification methods based on AERONET version 3 product over eastern Mediterranean and Black Sea. *Atmos. Pollut. Res.* **2020**, *11*, 2226–2243. [CrossRef]
67. Schmeisser, L.; Andrews, E.; Ogren, J.A.; Sheridan, P.; Jefferson, A.; Sharma, S.; Kim, J.E.; Sherman, J.P.; Sorribas, M.; Kalapov, I.; et al. Classifying aerosol type using in situ surface spectral aerosol optical properties. *Atmos. Chem. Phys.* **2017**, *17*, 12097–12120. [CrossRef]
68. Su, T.; Li, Z.; Zheng, Y.; Wu, T.; Wu, H.; Guo, J. Aerosol-boundary layer interaction modulated entrainment process. *NPJ Clim. Atmos. Sci.* **2022**, *5*, 64. [CrossRef]
69. Su, T.; Li, Z.; Li, C.; Li, J.; Han, W.; Shen, C.; Tan, W.; Wei, J.; Guo, J. The significant impact of aerosol vertical structure on lower atmosphere stability and its critical role in aerosol–planetary boundary layer (PBL) interactions. *Atmos. Chem. Phys.* **2020**, *20*, 3713–3724. [CrossRef]